Journal of
Mechanics of
Materials and Structures

IMPLICATIONS OF SHAKEDOWN FOR DESIGN OF ACTIVELY COOLED THERMOSTRUCTURAL PANELS

Natasha Vermaak, Lorenzo Valdevit, Anthony G. Evans, Frank W. Zok
and Robert M. McMeeking

Volume 6, No. 9-10 November–December 2011

mathematical sciences publishers

JOURNAL OF MECHANICS OF MATERIALS AND STRUCTURES
Vol. 6, No. 9-10, 2011

msp

IMPLICATIONS OF SHAKEDOWN FOR DESIGN OF ACTIVELY COOLED THERMOSTRUCTURAL PANELS

NATASHA VERMAAK, LORENZO VALDEVIT, ANTHONY G. EVANS,
FRANK W. ZOK AND ROBERT M. MCMEEKING

Propulsion systems in future hypersonic vehicles will require use of actively cooled structures that can withstand extreme thermomechanical loads. Candidate designs and materials for such structures have previously been identified through conventional yield-based design principles. The present article outlines an approach that utilizes concepts of localized plasticity and shakedown under cyclic loading in the design process. For this purpose, an established computational technique is used to determine shakedown limits for prototypical cooled structures. The results are employed in a design sensitivity study. The study demonstrates that, by allowing for shakedown, structures with areal densities significantly lower than those obtained from yield-limited design can be obtained. The magnitude of the benefits depends on the specific geometry of interest, the thermomechanical boundary conditions and the constraints placed on the design.

1. Introduction

The operating conditions of scramjet engines require use of lightweight materials that can withstand extreme heat fluxes and structural loads. They also demand designs that incorporate active cooling by the fuel. Previous studies on the design of thermostructural panels for scramjet engine liners have been based on established yield-limited design principles, i.e., with allowable stresses up to (but not exceeding) that required for yielding at the most critically stressed point in the structure [Heiser and Pratt 1994; Buchmann 1979; Scotti et al. 1988; Youn and Mills 1995; Flieder et al. 1971; Valdevit et al. 2008]. Building upon this body of work, the present study integrates concepts of local plasticity and thermomechanical shakedown into the design strategy. The objective is to reduce the structural weight. The rationale is that allowing the stresses to locally exceed the yield strength of the material upon the first few cycles, with fully elastic response thereafter (shakedown), can result in substantially lighter designs. For this purpose, a simplified technique [Abdalla et al. 2007] is used to conduct numerical Bree-like analysis [Bree 1967] of prospective geometries and determine shakedown limits, defined by critical combinations of thermal and mechanical stresses. The geometries selected for numerical analysis are obtained from previous optimizations based on yield-limited design [Valdevit et al. 2008]. The numerical analysis is used in combination with analytical models for stress and temperature predictions to identify designs that yield structures that are lighter than those found by yield-limited optimization yet lie within the shakedown regime.

Figure 1, left, depicts the notional combustor liner of present interest. The liner consists of four panels, three of which are shown in a rectangular configuration in the figure; each panel has rectangular cooling

Keywords: shakedown, lightweight structures, elastoplastic design, thermostructural panels.

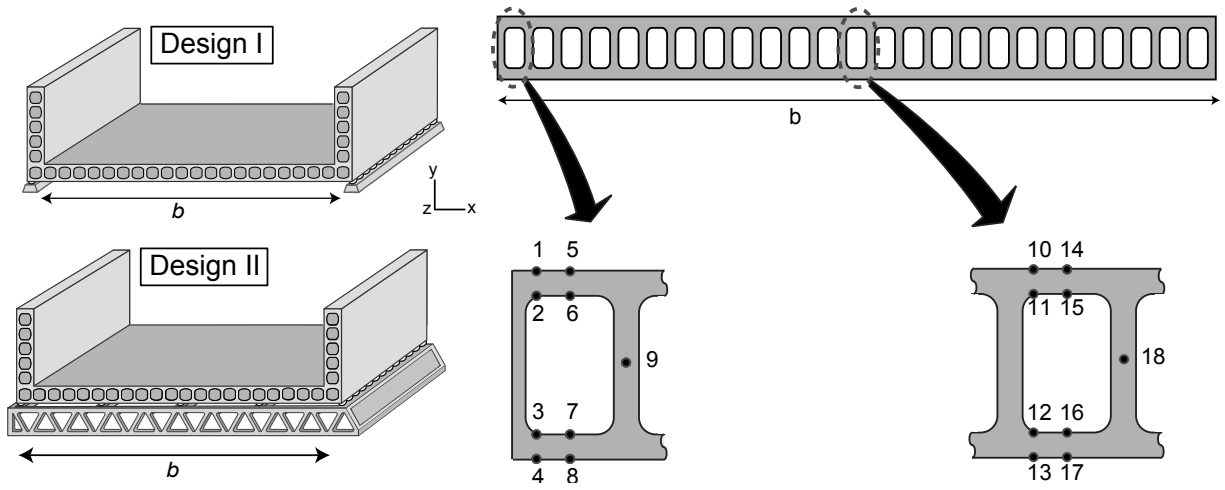

Figure 1. Left: notional design of scramjet engine liner. The two designs are distinguished by the nature of the underlying structure: either periodic linear supports or continuous panel. Both are assumed to be connected to the liner via rollers, thereby allowing unconstrained lateral thermal expansion. Right: cross-section through the liner and the locations of the 18 points most susceptible to yielding and monitored in the optimization code.

channels. The principal mechanical loads are those due to the internal pressure of the cooling fuel and the external pressure from the combustion gas. The dominant thermal loads arise from temperature gradients across the panel, subject to mechanical constraints imposed by the external boundaries (detailed in Section 3.) [Vermaak et al. 2010]. These loads and the pertinent structural dimensions are summarized in Figure 2.

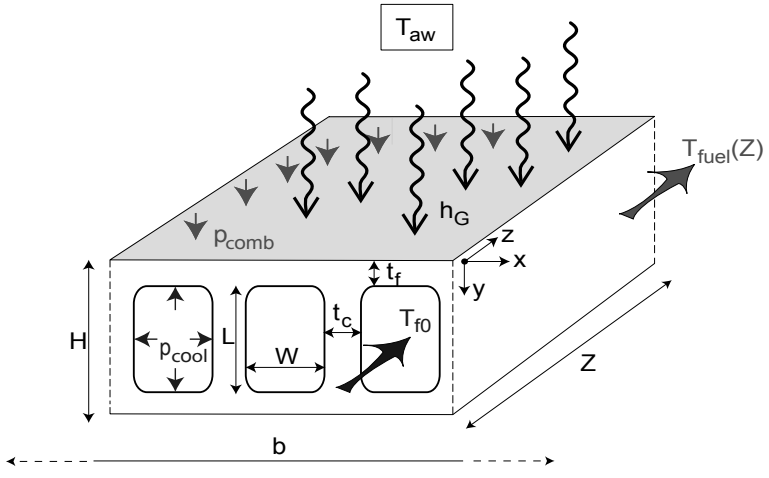

Figure 2. Schematic defining the geometry of the actively cooled panel, the pertinent dimensions, and the thermal and mechanical loads.

The article is organized as follows. First, the technique used to numerically determine shakedown limits is presented. Next, the use of the technique in the construction of a Bree diagram for a prototypical geometry is demonstrated. The results of a series of such computations are then used to identify optimal designs (with minimum mass) and their mass compared with those obtained through yield-limited optimizations. The weight benefits imparted by extending the design from yield-limited to shakedown-limited are computed for two types of external boundary conditions on the panel.

2. Construction of Bree diagrams

The classic problem. Bree diagrams [Bree 1967] have been used extensively in the nuclear pressure vessel industry to delineate the boundaries between various elastoplastic regimes. In the classic Bree problem, a thin-walled cylinder of an elastic, perfectly plastic material (see inset in Figure 3) is subjected to a fixed internal pressure, P, and a cyclic radial temperature difference ΔT between the inside and

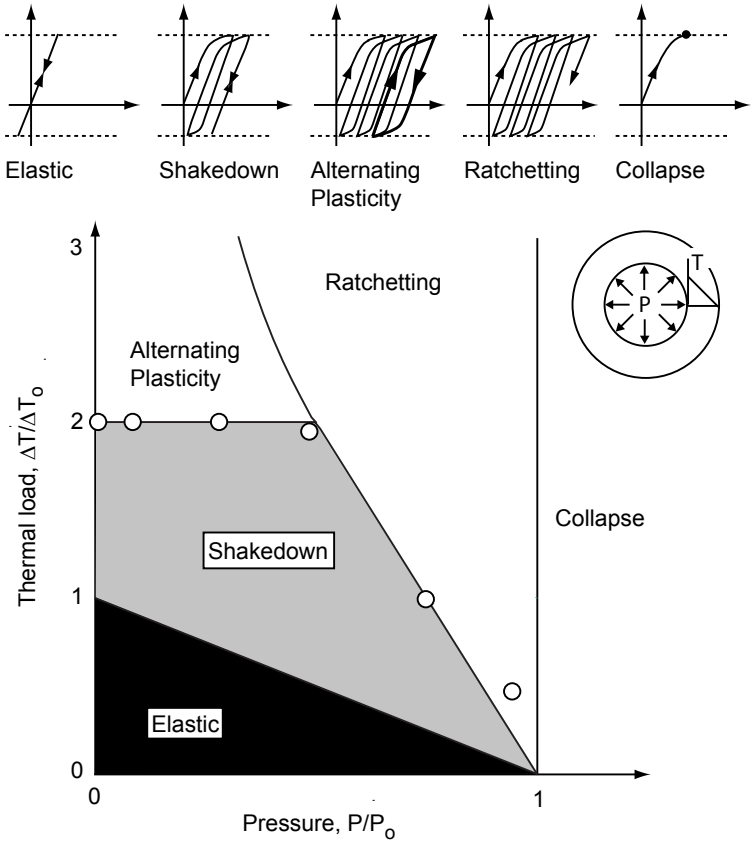

Figure 3. Top: prototypical stress-strain behaviors for an elastic-plastic material in the classic Bree problem. Bottom: the corresponding analytic Bree diagram. The fuel can is modeled as a cylindrical pressure vessel subject to constant internal pressure and a cyclic thermal gradient through the wall thickness. Data points represent FE calculations of the shakedown limit reported in [Abdalla et al. 2007].

outside walls.[1] The resulting Bree diagram is shown in Figure 3, bottom. The ordinate is $\Delta T/\Delta T_0$, where ΔT_0 is the temperature difference required for yield initiation in the absence of a mechanical load; the abscissa is P/P_0 with P_0 being the pressure that causes yielding in the absence of a temperature gradient.

For this configuration, the elastic domain is defined by $P/P_0 + \Delta T/\Delta T_0 < 1$. At one extreme, where $P/P_0 > 1$, *plastic collapse* occurs on the first load cycle. For intermediate combinations of P and ΔT, one of three behaviors is obtained (Figure 3) [Abdel-Karim 2005].

(1) In the *shakedown* regime, localized plastic deformation that occurs in the early stages of cycling gives rise to residual stresses that stabilize the plastic deformation. The consequence is purely elastic behavior during further loading cycles.

(2) *Alternating plasticity* occurs by loading beyond the shakedown limit. Here the plastic strain increment obtained during the first half of each loading cycle is followed by a plastic strain increment of equal magnitude but opposite sign during the second half. No net strain accrues during each cycle but the structure ultimately fails by low-cycle fatigue.

(3) *Ratcheting* refers to the condition in which a net increment of plastic strain accumulates during each cycle, eventually causing plastic collapse.

Computational approach. Although Bree diagrams can be constructed for simple geometries and loading conditions using analytical models [Bree 1967], numerical techniques are generally required [Abdel-Karim 2005]. In the present study, finite element analysis (FEA) is used to apply a methodology initially reported in [Abdalla et al. 2007]. The approach yields an estimate of the shakedown limit in accordance with Melan's lower bound theorem[2]. The theorem states that a structure will shakedown if a time-independent residual stress field can be found which satisfies mechanical equilibrium and the boundary conditions and the combined residual and elastic stresses do not exceed yield at any time during the loading cycle [König 1987; Bower 2009].

For implementation, the methodology requires two sets of computations for each geometry. In the first, the stresses caused by the cyclic load in an *elastic* structure are computed. This analysis is performed only once and its output stored. The second is an elastic-plastic analysis, assuming perfectly plastic behavior beyond yield, incorporating both the time-invariant and the cyclic loads in consecutive steps. The time-invariant load is applied first to a specified level and a half cycle of the varying load is then applied to its specified level. Each is incremented monotonically from zero to its peak value while an elastic-plastic analysis is carried out. Residual stresses are then calculated at every material point in accordance with

$$\sigma_{r,n} = \sigma_{\mathrm{EP},n} - \sigma_E \frac{\Delta C_n}{\Delta C_{\mathrm{ref}}}, \tag{1}$$

where σ_E and ΔC_{ref} are the stress tensor and cyclic load amplitude for the elastic analysis and $\sigma_{\mathrm{EP},n}$ and ΔC_n are the corresponding values for the stress tensor and cyclic load amplitude resulting from the n-th trial calculation in the elastic-plastic analysis [Abdalla et al. 2007]. If the effective (von Mises) residual

[1] Subsequently, the effects of alternative loading sequences (e.g., in-phase versus out-of-phase) were also investigated [Ng and Moreton 1983].

[2] The Melan theorem and all analyses presented herein assume elastic perfectly plastic material behavior.

stresses lie inside the yield surface at every point in the structure, the n-th combination of time-invariant and cyclic loads constitute a lower bound to the shakedown limit. The process is repeated for progressively increasing time-invariant and cyclic loads until yield is just reached by the resulting effective residual stress. The associated combination of time-invariant and cyclic loads represents one point on the shakedown curve on the Bree diagram. The computations are repeated for other load combinations until the full shakedown boundary is obtained over the domain of interest. Results obtained in [Abdalla et al. 2007] for the classic Bree problem are reported in Figure 3.

Implementation for actively cooled combustor liner. The Bree diagram for a representative unit cell of an actively cooled panel was constructed in accordance with the preceding prescription. The cell geometry and dimensions (depicted in Figure 4) were obtained from a yield-limited optimization analysis reported in an earlier study [Valdevit et al. 2008]. Here the internal pressure within the channels is assumed to be time-invariant. The thermal load (assumed cyclic) consists of a uniform temperature difference between the two faces (denoted "hot" and "cold"). Uniform thermal expansion in the lateral (x_1) direction (without bending) is permitted. The selection of the internal pressure as the time-invariant load and the temperature difference as the cyclic load is consistent with Bree's original analysis.

All computations were performed using the ABAQUS© finite element code. The mesh consisted of bi-quadratic generalized plane strain elements with reduced integration and hybrid formulation (CPEG8RH). The radius of the corner fillet in the finite element analysis was taken to be 0.1 mm, representative of that obtained through electrical discharge machining (EDM) when a nominally square corner is prescribed. (The resulting radius is dictated largely by the diameter of the EDM wire.) This fillet value also represents the most conservative design as smaller fillets are not feasible by EDM (or any other reasonable

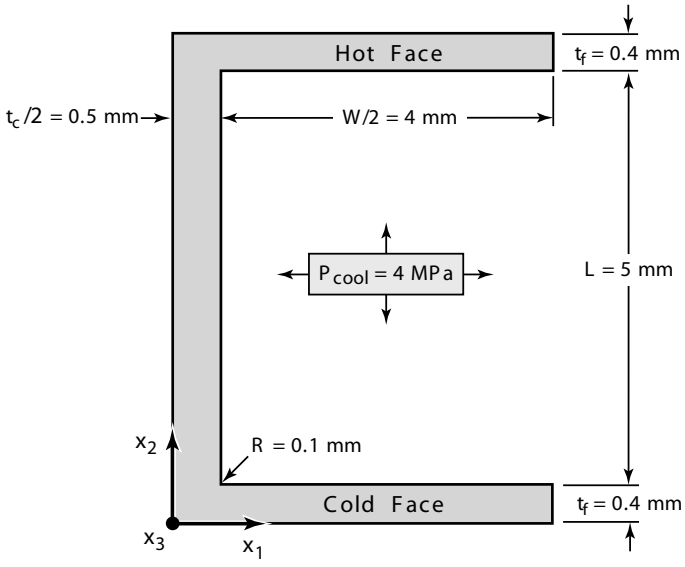

Figure 4. The half unit cell used in the finite element computations for construction of the Bree diagram in Figure 5. This particular geometry emerged as being nearly optimal for a yield-limited design. The boundary conditions are defined by: $u_1 = 0$ along $x_1 = 0$, $u_2 = 0$ along $x_2 = 0$, and $u_1 =$ constant along $x_1 = (W + t_c)/2$ (u being displacement).

	Inconel X-750	C-SiC
Upper use temperature, T^* (K)	1100	1810
Yield strength, σ_0 (at T^*) (MPa)	527	400
Temperature dependence of strength, $d\sigma_0/dT$ (MPa/K)	-0.4	—
Young's modulus, E (GPa)	130	140
Thermal expansion coefficient, α ($10^{-6}\,\mathrm{K}^{-1}$)	16	2
Thermal conductivity, k (W/mK)	23	15 (in-plane) 5 (through-thickness)
Density, ρ (kg/m^3)	8280	2000

Table 1. Thermomechanical properties of candidate materials.

manufacturing approach) and larger fillets will relax stress concentrations. The material properties were selected to be representative of Inconel X-750 (Table 1).

Elastic-plastic computations were performed for coolant pressures P ranging from zero to that needed to exceed the shakedown boundary in the absence of a thermal load. For presentation on a Bree diagram, the pressure was normalized by the *nominal* value P_0 required for first yield, obtained by modeling the face-sheet as a uniformly loaded edge-clamped plate under plane strain conditions. The result is (see [Valdevit et al. 2008; Beer and Johnston 1981])

$$P_0 = \frac{4}{\sqrt{3}}\sigma_0\left(\frac{t_f}{W}\right)^2, \tag{2}$$

where W is the channel width and t_f the face-sheet thickness (Figure 4). The value of P_0 obtained from the finite element analysis is somewhat lower than that calculated from (2), by about 30%. The nonconservative nature of the analytical prediction is due to the stress concentrations that arise at the corners in the finite element analysis but are neglected in the plate model.

At each pressure level, the temperature difference ΔT between the faces was incremented to ascertain both the first yield and the shakedown boundaries.[3] (No attempt was made to differentiate the elasto-plastic deformation modes beyond the shakedown limit, as they would all be equally unacceptable for the application under consideration.) This temperature difference was normalized by the critical value needed for yield initiation, calculated using the analytical solution presented in the Appendix.

The resulting Bree diagram is shown in Figure 5. It exhibits elastic and shakedown boundaries that are qualitatively similar to those in Figure 3 (though without the specific plasticity modes beyond the shakedown limit). While the classic Bree diagram for the thin-walled *cylindrical* pressure vessel is universally applicable to all such vessels subjected to the same sequence of loading conditions, the *rectangular* geometry of the present combustor panels precludes interpretation of Figure 5 as a similarly universal result. That is, the Melan theorem requirements are not automatically satisfied when the unit-cell geometry of the combustor panel is changed. Consequently, the Bree diagram in Figure 5 is specific

[3] In the FEA, conditions are checked at integration stations of the elements and the component is deemed to shakedown if all integration stations pass the test of not violating yield.

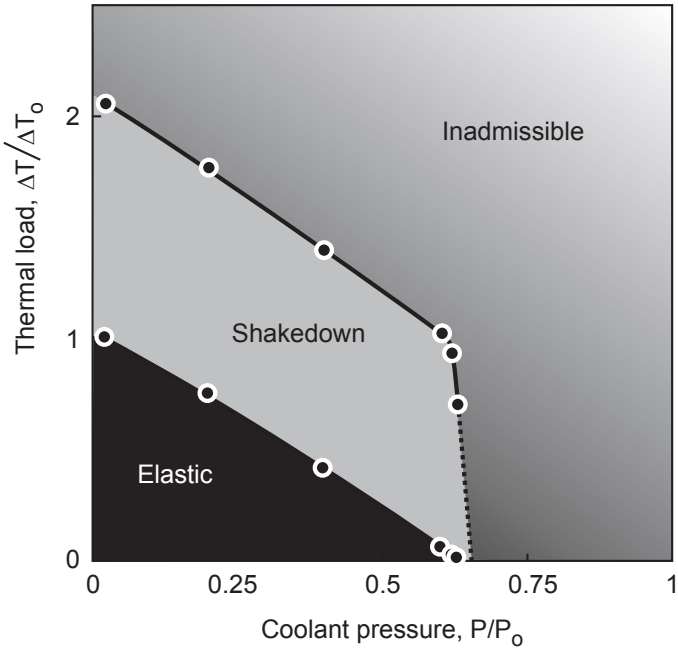

Figure 5. The Bree diagram for the combustor panel, based on analyses of the unit cell in Figure 4. Elastoplastic behaviors beyond shakedown (ratcheting, cyclic plasticity and plastic collapse) are considered inadmissible.

to the geometry depicted in Figure 4. Strictly, in order to utilize such results in an optimization code, computations of this kind would need to be performed for all possible geometries. The computational effort for this task would be prohibitive.

In light of these limitations, the shakedown concept was employed in the optimization in the following way. First, the dimensions of the optimal yield-limited design were obtained using the algorithm presented in [Valdevit et al. 2008] and summarized in Section 3. Then, the dimensions were incrementally varied in a manner that yielded a mass reduction and the shakedown limit was numerically computed. The process was repeated until the resulting structure was no longer within the shakedown limit. Comparisons of the mass of the penultimate structure with that of the yield-limited design were used to assess the benefits of extending the design into the shakedown domain. The following section describes the protocol used to determine optimal yield-limited designs. It also describes how these designs were varied in a sensitivity study to find lighter weight solutions subject to the shakedown limit.

3. Sensitivity study procedure

The reference [Valdevit et al. 2008] may be consulted for details not given in this section.

Optimal yield-or-fracture-limited designs. The optimization protocol was applied to two representative combustor panel support conditions (Figure 1). In Design I, periodic line supports are placed along the panel base. Panel-level bending stresses ensue between the supports due to the combustion pressure. In Design II, a supporting panel is attached to the base, preventing panel-level bending. Isotropic thermal

expansion is permitted in both designs. The essential difference between the designs is that, in Design II, the combustion pressure is rendered inconsequential, reducing the dominant loads to two: the coolant pressure and the panel level thermal gradient. In contrast, three loads remain for Design I.

The optimization protocol consists of the following steps. The values of heat load and fuel flow rate are identified for the specified vehicle Mach number, assumed to be 7. The heat load is characterized by the temperature difference between the combustion gas (specifically, the adiabatic wall temperature, $T_{\text{aw}} = 3050\,\text{K}$) and the hot surface (evaluated analytically) and the corresponding heat transfer coefficient, h_G. The latter was computed assuming steady-state combustion conditions, yielding $h_G = 445\,\text{W/m}^2\text{K}$. The fuel flow rate through the cooling channels was taken to be that for stoichiometric combustion of the fuel with the available oxygen in the flowpath. The (internal) pressure in the cooling channels is set by injection requirements ($p_{\text{cool}} = 4\,\text{MPa}$ for a prototypical vehicle), and the (external) combustion chamber pressure is obtained by the flow conditions in the combustor ($p_{\text{comb}} = 0.16\,\text{MPa}$ for Mach 7 conditions). The design parameters are incrementally varied over a prescribed range and the pertinent stresses and temperatures were computed. (In principle, the heat transfer coefficient can be increased to reflect local heat spikes due to nonuniform combustion and the flow rate varied relative to the stoichiometric value. Variations in these parameters were not considered in the present study.)

Temperature distributions were obtained by means of a thermal network model. The stresses due to both the coolant pressure and the temperature gradients were obtained at critical locations using standard thermoelastic plate analysis. A synopsis of the models for the temperature and stress distributions is presented in the Appendix. Upon comparison of the computed stresses and temperatures with the corresponding material and coolant properties, the viability of the design is ascertained.

Specifically, for viability in the case of metallic candidates that are *yield-limited*, the effective (von Mises) stress must not exceed the yield stress anywhere in the structure. Similarly, for ceramic matrix composite (CMC) candidates such as C/SiC, *fracture-limited* design is determined by ensuring that the maximum and minimum principal stresses in the structure remain below/above critical values ($\pm 400\,\text{MPa}$ for C/SiC).

Additionally, for all candidates the fuel temperature must not exceed that for coking (975 K for JP-7) and the maximum material temperature must not exceed its upper use (softening) temperature (1100 K for Inconel X-750). If solutions exist, the design is optimized for minimum mass, Additionally, to ensure realistic designs, constraints based on panel manufacturability and fuel pressure drop were also prescribed. For instance, to enable manufacturing of the panels by conventional means, minimum values were prescribed for the face and core member thicknesses (0.4 mm), the channel height (5 mm) and the channel width (2 mm). Numerical optimizations were performed using the quadratic optimizer MINCON in MATLAB. The process was repeated using several different randomly generated initial guesses to ensure the optimized solutions were not in local minima.

Probing benefits of shakedown. Two slightly different schemes were employed to calculate the operational conditions associated with the two sets of boundary conditions (defined by Designs I and II) and assess whether they reside within the shakedown limit. The scheme for Design II is straightforward. The internal pressure is selected to be 4 MPa and the operational temperature difference, ΔT_{panel}, is calculated from the thermal network model (Appendix). Comparisons of ΔT_{panel} with the shakedown value (calculated by FEA) determine the viability of the structure.

For Design I, an additional calculation is required to account for the combustion pressure in the Bree analysis. Since the panel acts essentially as a clamped plate that bends between the supports, the combustion pressure produces uniform tensile or compressive stresses in the face sheets normal to the direction of the underlying supports. These uniform stresses are of the same form as those arising from the thermal load. Additionally, both are operative at the same time, i.e., during combustion. Consequently, from a mathematical viewpoint, the two loads can be represented by an effective (fictitious) temperature change, ΔT_{eff}, that produces the same stresses in the face sheets. The stresses are obtained in the following way.

From an analysis of a plate under generalized plane strain conditions, the stresses induced by the *real* temperature difference ΔT_{panel} are given by

$$\sigma_{xx}^{\Delta T_{\text{panel}}} = \begin{cases} -\dfrac{E\alpha\Delta T_{\text{panel}}}{2(1-\nu)} & \text{in the hot face,} \\ \dfrac{E\alpha\Delta T_{\text{panel}}}{2(1-\nu)} & \text{in the cold face,} \end{cases}$$

$$\sigma_{zz}^{\Delta T_{\text{panel}}} = \begin{cases} \left[\dfrac{-E\alpha\Delta T_{\text{panel}}}{2(1-\nu)}\right]\left[\dfrac{(2-\nu)Lt_c + 2t_f(W+t_c)}{Lt_c + 2t_f(W+t_c)}\right] & \text{in the hot face,} \\ \left[\dfrac{E\alpha\Delta T_{\text{panel}}}{2(1-\nu)}\right]\left[\dfrac{\nu Lt_c + 2t_f(W+t_c)}{Lt_c + 2t_f(W+t_c)}\right] & \text{in the cold face.} \end{cases} \tag{3}$$

From an analogous plate bending analysis, the stresses caused by the combustion pressure are

$$\sigma_{xx}^{p_{\text{comb}}} = \begin{cases} p_{\text{comb}}\dfrac{1}{12}\dfrac{b^2}{(L+t_f)t_f} & \text{at points 1, 2, 5, 6,} \\ -p_{\text{comb}}\dfrac{1}{12}\dfrac{b^2}{(L+t_f)t_f} & \text{at points 3, 4, 7, 8,} \\ p_{\text{comb}}\dfrac{1}{24}\dfrac{b^2}{(L+t_f)t_f} & \text{at points 12, 13, 16, 17,} \\ -p_{\text{comb}}\dfrac{1}{24}\dfrac{b^2}{(L+t_f)t_f} & \text{at points 10, 11, 14, 15,} \end{cases} \tag{4}$$

$$\sigma_{zz}^{p_{\text{comb}}} = \nu\sigma_{xx}^{p_{\text{comb}}} \quad \text{at all points.}$$

where b is the distance between supports (assumed to be 0.5 m) and the points 1–17, defined on Figure 1, right, represent critical locations where stress combinations are most severe. The stress components in (3) and (4) are added at every point and the von Mises stress $\bar{\sigma}(\Delta T_{\text{panel}}, p_{\text{comb}})$ obtained in the usual manner:

$$\bar{\sigma}(\Delta T_{\text{panel}}, p_{\text{comb}}) = \sqrt{\tfrac{1}{2}\left(\sigma_{xx}^2 + \sigma_{zz}^2 + (\sigma_{xx} - \sigma_{zz})^2\right)}. \tag{5}$$

The stresses produced by the *effective* temperature difference are of similar form to those in (3), with ΔT_{panel} replaced by ΔT_{eff}, yielding

$$\sigma_{xx}^{\Delta T_{\text{eff}}} = \begin{cases} -\dfrac{E\alpha\Delta T_{\text{eff}}}{2(1-\nu)} & \text{in the hot face,} \\ \dfrac{E\alpha\Delta T_{\text{eff}}}{2(1-\nu)} & \text{in the cold face,} \end{cases} \tag{6a}$$

$$\sigma_{zz}^{\Delta T_{\text{eff}}} = \begin{cases} \left[\dfrac{-E\alpha\Delta T_{\text{eff}}}{2(1-\nu)}\right]\left[\dfrac{(2-\nu)Lt_c + 2t_f(W+t_c)}{Lt_c + 2t_f(W+t_c)}\right] & \text{in the hot face,} \\ \left[\dfrac{E\alpha\Delta T_{\text{eff}}}{2(1-\nu)}\right]\left[\dfrac{\nu Lt_c + 2t_f(W+t_c)}{Lt_c + 2t_f(W+t_c)}\right] & \text{in the cold face.} \end{cases} \tag{6b}$$

The corresponding effective stress is

$$\bar{\sigma}(\Delta T_{\text{eff}}) = \sqrt{\tfrac{1}{2}\left[\left(\sigma_{xx}^{\Delta T_{\text{eff}}}\right)^2 + (\sigma_{zz}^{\Delta T_{\text{eff}}})^2 + (\sigma_{xx}^{\Delta T_{\text{eff}}} - \sigma_{zz}^{\Delta T_{\text{eff}}})^2\right]}. \tag{7}$$

The effective temperature difference is obtained by setting $\bar{\sigma}(\Delta T_{\text{panel}}, p_{\text{comb}}) = \bar{\sigma}(\Delta T_{\text{eff}})$ — see Equations (5) and (7) — and numerically inverting the result to obtain $\Delta T_{\text{eff}}(\Delta T_{\text{panel}}, p_{\text{comb}})$. The viability of a design is ascertained by comparing ΔT_{eff} with the shakedown limit computed by FEA.

4. Designs allowing shakedown

The key results of the sensitivity study are summarized in Figure 6 for Designs I and II. The figure illustrates the benefits associated with designing to shakedown, characterized by the ratio of minimum panel masses. Also shown in Figure 6 is the panel mass for an optimized C/SiC composite. (This result is based on a fracture-limited design, using criteria based on critical values of the maximum and minimum principal stresses. Shakedown is not considered in this case since the underlying plasticity mechanisms

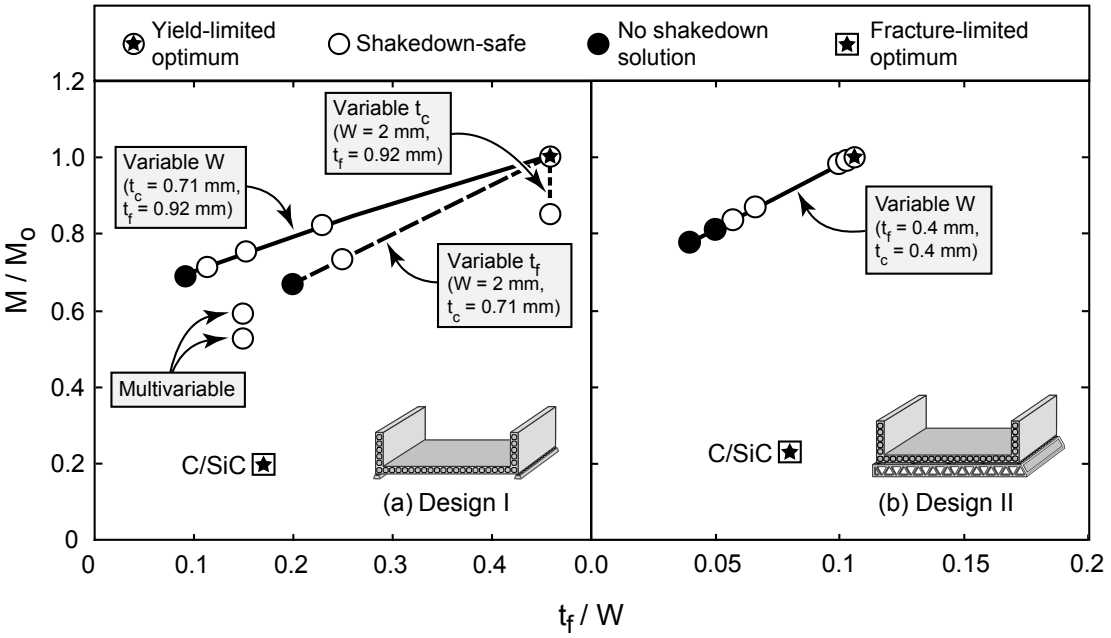

Figure 6. Benefits of shakedown-limited design in the minimum mass of an actively cooled Inconel X-750 panel under the two design scenarios. Here M_0 is the mass of the optimal yield-limited design. For all Inconel solutions, channel height, L, is at the minimum value (5 mm). Also shown for comparison are the results for the fracture-limited optimum for a C/SiC composite.

	Design I												Design II						
	C/SiC	Inconel X-750											C/SiC	Inconel X-750					
L	10.71	5	5	5	5	5	5	5	5	5	5	5	5	5	5	5	5	5	5
W	5.11	2	2	2	4	6	8	10	2	4	4	4	4.97	3.77	4	6	7	8	10
t_f	0.87	0.92	0.5	0.4	0.92	0.92	0.92	0.92	0.92	0.6	0.6	0.4	0.4	0.4	0.4	0.4	0.4	0.4	0.4
t_c	0.4	0.71	0.71	0.71	0.71	0.71	0.71	0.71	0.4	0.6	0.4	0.4	0.4	0.4	0.4	0.4	0.4	0.4	0.4
M/M_0	0.2	1	0.73	–	0.82	0.75	0.71	–	0.85	0.59	0.53	–	0.22	1	0.98	0.87	0.84	–	–
	FL	YL	SL	–	SL	SL	SL	–	SL	SL	SL	–	FL	YL	SL	SL	SL	–	–

Table 2. Geometries for design optimization and shakedown analyses. Abbreviations on the last row stand for fracture-limited (FY), yield-limited (YL), and shakedown-limited (SL). A dash on the last two rows indicates no solution. The geometric parameters L, W, t_f, and t_c are given in units of mm.

are not operative in these materials at the temperatures of interest.) For consistency, the C/SiC panel mass is also normalized by that of the optimized Inconel X-750 structure. Previous optimization studies have revealed C/SiC to yield the lightest structure and it is thus used as a benchmark against which the metallic designs are assessed.

Evidently the benefits of incorporating shakedown depend sensitively on the boundary conditions. For instance, for Design II, the optimal face sheet and core member thicknesses as well as channel height are already at their minimum allowable values in the yield-limited design (Table 2). Consequently, they cannot be reduced further to take advantage of the shakedown phenomenon. The only available avenue for weight reduction is to increase the channel width, W, from its optimal value of 3.8 mm. The results from a number of FEA computations for several values of W are summarized in Table 2 and plotted on Figure 6. In this case, the shakedown limit is breached when W exceeds 7 mm. The resulting weight reduction is modest (about 16%).

For Design I, incorporating shakedown yields greater benefits in mass reduction. In this case, among the free geometric variables, only the channel height, L, is at its minimum allowable value for the optimal yield-limited design. Consequently, computations were performed for lower values of face sheet and core member thicknesses as well as higher values of channel width. The results in Figure 6(a) are labeled accordingly. While each of these changes results in some mass reduction, the magnitudes of the contributions differ. For example, decreasing t_c from 0.71 mm to its minimum allowable value (0.4 mm) while maintaining all other parameters fixed yields a mass reduction of 15%. Mass reductions of 27% and 29% are obtained for reduced values of t_f (from 0.92 mm to 0.5 mm) and elevated values of W (from 2 mm to 8 mm), respectively. The greatest benefits are obtained by varying the three dimensions simultaneously. Among the cases considered here (Table 2), the best one produces a nearly 50% reduction in mass.

Even exploiting shakedown in the design of the Inconel X-750 structure, its mass is still about 2.7 times that of the optimized C/SiC structure. But, because of the relative ease of manufacturing metallic

components along with their superior structural robustness, the metallic alloy may prove to be preferable to the ceramic composite for the present application.

While the present shakedown analysis demonstrates potential weight savings, additional research is required to provide more insight into the physical behavior of such structures. Particularly, their response in competition with creep environments is of interest. The computational approach presented provides a working limit for shakedown that motivates the development of complementary models of material behavior during structural shakedown.

5. Conclusions

Incorporating shakedown into the design of actively cooled thermostructural panels can enable significant weight reduction. The magnitude of the benefit depends on the component of interest, the boundary conditions and the specific constraints placed on the design. For the component considered here — a liner for a scramjet engine operating at stoichiometric fuel flow rates under steady-state combustion conditions for Mach 7 flight — significant benefits accrue only when the liner is weakly supported by an external structure. Otherwise, when the support structure provides a more substantial constraint on deformation, the design is influenced more heavily by the material softening temperature and the secondary constraints derived from manufacturing limitations than by the thermomechanical loads. In such cases, the more aggressive design strategy, exploiting shakedown, is of minimal benefit.

Appendix: Synopsis of analytical models

Temperature distributions. Analytical expressions for the temperatures at critical locations in the panel have been obtained via a thermal network approach, subject to four simplifying assumptions:

(1) T_{aw} and h_G are uniform along the hot face;

(2) all heat is removed by forced convection in the cooling channels;

(3) longitudinal panel conduction is negligible so that the gradient of hot surface temperature in the fuel flow direction is due only to cooling into the fuel channel; and

(4) the coolant temperature, due to turbulent mixing, is uniform across the channel cross-section.

Based on the thermal network in Figure 7, the temperature in the fluid is:

$$T_f = T_{\text{aw}} - (T_{\text{aw}} - T_f^0) \cdot \exp(-\beta z) \tag{A.1}$$

and the temperature distributions at the 18 locations depicted in Figure 1 are:

$$T^{(i)} = T_{\text{aw}} - (T_{\text{aw}} - T_f^0) \cdot F^{(i)} \exp(-\beta z) \tag{A.2}$$

where $F^{(i)}$ and β depend on: the geometry of the panel (W, L, t_f, t_c); the thermal conductivity of the material, k_s; the thermal conductivity, k_f, kinematic viscosity, ν_f, and volumetric specific heat, $\rho_f c_{p,f}$, of the fuel; the heat transfer coefficient on the hot side, h_G; and the volumetric fuel flow rate, $\dot{V}$ (see [Valdevit et al. 2008] for details). Importantly, these functional dependencies are intertwined, thus precluding straightforward interpretation of the effect of each quantity on the temperature distribution.

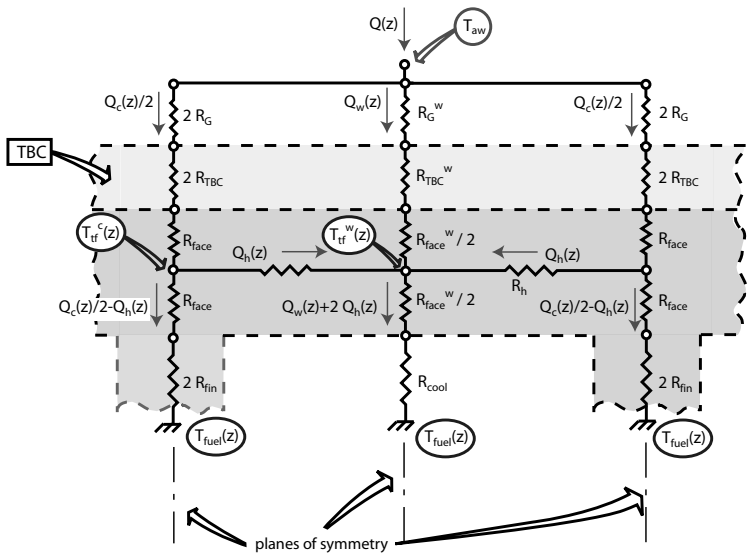

OVER THE WEB	$R_G = \frac{1}{h_G t_c}$	$R_{TBC} = \frac{t_{TBC}}{k^{\perp}_{TBC} t_c}$	$R_{face} = \frac{t_f}{k^{\perp}_s t_c}$	$R_{fin} = \frac{\tanh^{1} \sqrt{2h_c / k^{\parallel}_s t_c}\, L}{\sqrt{2h_c / k^{\parallel}_s t_c}\, k^{\parallel}_s t_c}$	$R_h = \frac{W \quad t_c/2}{4 k^{\parallel}_s t_f}$
BETWEEN WEBS	$R^w_G = \frac{t_c}{W} R_G$	$R^w_{TBC} = \frac{t_c}{W} R_{TBC}$	$R^w_{face} = \frac{t_c}{W} R_{face}$	$R_{cool} = \frac{1}{h_c W}$	

Figure 7. Thermal resistance network used to determine temperature distributions, along with expressions for all relevant thermal resistances.

The dominant thermal stresses in the panel depend on the temperature difference between the two faces $\Delta T_{\text{panel}}(z)$. For simplicity, this difference is averaged in the x-direction, and can be expressed as:

$$\Delta T_{\text{panel}}(z) = (T_{\text{aw}} - T_f^0) \cdot G_1 \cdot \exp(-\beta z) \tag{A.3}$$

where G_1 depends on the same quantities as $F^{(i)}$.

The accuracy of this analytical model has been verified with a number of selected computational fluid dynamics and FEA computations; the temperature distributions are generally captured by (A.2) to within $\sim 1\%$ and the temperature gradient captured by (A.3) to within $\sim 8\%$ [Valdevit et al. 2008].

Stress distributions. The dominant stresses are induced by the combustion chamber pressure, p_{comb}, on the hot side of the panel, the fuel pressure, p_{cool}, inside the cooling channels, and the temperature difference, ΔT_{panel}, between the hot and cold faces. Assuming generalized plane strain conditions (with no rotation about the x and y axes), the mechanical stresses (membrane plus bending) at each of the 18 locations depicted in Figure 1 are given by

$$\sigma^{(i)}_{m,x} = A^{(i)} p_{\text{cool}} + B^{(i)} p_{\text{comb}}, \quad \sigma^{(i)}_{m,z} = \nu \sigma^{(i)}_{m,x} \tag{A.4}$$

where the functions $A^{(i)}$, $B^{(i)}$ depend on panel geometry and support conditions and ν is Poisson's ratio. Similarly, the dominant thermal stresses can be expressed as:

$$\sigma_{T,x}^{(i)} = \frac{E\alpha}{1-\nu}(D_x^{(i)}\Delta T_{\text{panel}}^{(i)}), \quad \sigma_{T,z}^{(i)} = \frac{E\alpha}{1-\nu}(D_z^{(i)}\Delta T_{\text{panel}}^{(i)}), \tag{A.5}$$

where E and α are the Young's modulus and the coefficient of thermal expansion, respectively. The quantities $D_x^{(i)}$ and $D_z^{(i)}$ are functions of geometry only. Additional details are presented in [Valdevit et al. 2008]. The accuracy of this model has been verified with FEA. Its accuracy is better than $\sim 10\%$ on the top face and $\sim 20\%$ on the bottom face (*loc. cit.*).

Acknowledgements

This work was supported by the Office of Naval Research through the Multidisciplinary University Research Initiative program on Revolutionary Materials for Hypersonic Flight (Contract N00014-05-1-0439, Program Manager Dr. J. Christodoulou). Computing time on a HP Opteron cluster was provided by the California NanoSystems Institute at the University of California, Santa Barbara and by Hewlett-Packard. Helpful correspondence with and advice from Dr. H. F. Abdalla of The American University in Cairo is greatly appreciated.

References

[Abdalla et al. 2007] H. F. Abdalla, M. M. Megahed, and M. Y. A. Younan, "A simplified technique for shakedown limit load determination", *Nucl. Eng. Des.* **237**:12–13 (2007), 1231–1240.

[Abdel-Karim 2005] M. Abdel-Karim, "Shakedown of complex structures according to various hardening rules", *Int. J. Press. Vessels Pip.* **82**:6 (2005), 427–458.

[Beer and Johnston 1981] F. P. Beer and E. R. Johnston, *Mechanics of materials*, Chapter 7, McGraw-Hill, New York, 1981.

[Bower 2009] A. F. Bower, *Applied mechanics of solids*, Chapter 6, pp. 381–422, CRC Press, Boca Raton, FL, 2009, Available at http://www.solidmechanics.org.

[Bree 1967] J. Bree, "Elastic-plastic behaviour of thin tubes subjected to internal pressure and intermittent high-heat fluxes with application to fast-nuclear-reactor fuel elements", *J. Strain Anal. Eng. Des.* **2**:3 (1967), 226–238.

[Buchmann 1979] O. A. Buchmann, "Thermal-structural design study of an airframe-integrated scramjet", Contractor report NASA CR-3141, NASA, Washington, DC, 1979, Available at http://www.tinyurl.com/NASA-CR-3141.

[Flieder et al. 1971] W. C. Flieder, C. E. Richard, O. A. Buchmann, and F. M. Walters, "An analytical study of hydrogen cooled panels for application to hypersonic aircraft", Contractor report NASA CR-1650, NASA, Washington, DC, 1971, Available at http://www.tinyurl.com/NASA-CR-1650.

[Heiser and Pratt 1994] W. H. Heiser and D. T. Pratt, *Hypersonic airbreathing propulsion*, AIAA, Washington, DC, 1994.

[König 1987] J. A. König, *Shakedown of elastic-plastic structures*, Chapter 4, Fundamental Studies in Engineering **7**, Elsevier, Amsterdam, 1987.

[Ng and Moreton 1983] H. W. Ng and D. N. Moreton, "Bree diagrams for alternative loading sequences", pp. 279–312 in *Engineering approaches to high temperature design*, edited by B. Wilshire and D. R. J. Owen, Recent Advances in Creep and Fracture of Engineering Materials and Structures **2**, Pineridge Press, Swansea, 1983.

[Scotti et al. 1988] S. J. Scotti, C. J. Martin, and S. H. Lucas, "Active cooling design for scramjet engines using optimization methods", Technical memorandum NASA TM-100581, NASA Langley Research Center, Hampton, VA, 1988, Available at http://www.tinyurl.com/NASA-TM-100581.

[Valdevit et al. 2008] L. Valdevit, N. Vermaak, F. W. Zok, and A. G. Evans, "A materials selection protocol for lightweight actively cooled panels", *J. Appl. Mech.* (*ASME*) **75**:6 (2008), 061022.

[Vermaak et al. 2010] N. Vermaak, L. Valdevit, and A. G. Evans, "Influence of configuration on materials selection for actively cooled combustors", *J. Propuls. Power* **26**:2 (2010), 295–302.

[Youn and Mills 1995] B. Youn and A. F. Mills, "Cooling panel optimization for the active cooling system of a hypersonic aircraft", *J. Thermophys. Heat Transf.* **9**:1 (1995), 136–143.

Received 24 May 2011. Revised 28 Jul 2011. Accepted 8 Aug 2011.

NATASHA VERMAAK: natasha@engineering.ucsb.edu
Materials Department, University of California, Santa Barbara, CA 93106-5050, United States

LORENZO VALDEVIT: valdevit@uci.edu
Department of Mechanical and Aerospace Engineering and Department of Chemical Engineering and Materials Science, University of California, Irvine, CA 92697-3975, United States

ANTHONY G. EVANS: agevans@engineering.ucsb.edu
Materials Department, University of California, Santa Barbara, CA 93106-5050, United States
http://www.me.ucsb.edu/dept_site/people/evans_page.html

FRANK W. ZOK: zok@engineering.ucsb.edu
Materials Department, University of California, Santa Barbara, CA 93106-5050, United States
http://engineering.ucsb.edu/~zok/zok.html

ROBERT M. MCMEEKING: rmcm@engineering.ucsb.edu
Materials and Mechanical Engineering Departments, University of California, Santa Barbara, CA 93106-5050, United States

JOURNAL OF MECHANICS OF MATERIALS AND STRUCTURES

jomms.org

Founded by Charles R. Steele and Marie-Louise Steele

EDITORS

CHARLES R. STEELE	Stanford University, USA
DAVIDE BIGONI	University of Trento, Italy
IWONA JASIUK	University of Illinois at Urbana-Champaign, USA
YASUHIDE SHINDO	Tohoku University, Japan

EDITORIAL BOARD

H. D. BUI	École Polytechnique, France
J. P. CARTER	University of Sydney, Australia
R. M. CHRISTENSEN	Stanford University, USA
G. M. L. GLADWELL	University of Waterloo, Canada
D. H. HODGES	Georgia Institute of Technology, USA
J. HUTCHINSON	Harvard University, USA
C. HWU	National Cheng Kung University, Taiwan
B. L. KARIHALOO	University of Wales, UK
Y. Y. KIM	Seoul National University, Republic of Korea
Z. MROZ	Academy of Science, Poland
D. PAMPLONA	Universidade Católica do Rio de Janeiro, Brazil
M. B. RUBIN	Technion, Haifa, Israel
A. N. SHUPIKOV	Ukrainian Academy of Sciences, Ukraine
T. TARNAI	University Budapest, Hungary
F. Y. M. WAN	University of California, Irvine, USA
P. WRIGGERS	Universität Hannover, Germany
W. YANG	Tsinghua University, China
F. ZIEGLER	Technische Universität Wien, Austria

PRODUCTION contact@msp.org

SILVIO LEVY Scientific Editor

Cover design: Alex Scorpan Cover photo: Mando Gomez, www.mandolux.com

See http://jomms.org for submission guidelines.

JoMMS (ISSN 1559-3959) is published in 10 issues a year. The subscription price for 2011 is US $520/year for the electronic version, and $690/year (+$60 shipping outside the US) for print and electronic. Subscriptions, requests for back issues, and changes of address should be sent to Mathematical Sciences Publishers, Department of Mathematics, University of California, Berkeley, CA 94720–3840.

JoMMS peer-review and production is managed by EditFLOW® from Mathematical Sciences Publishers.

PUBLISHED BY
mathematical sciences publishers
http://msp.org/

A NON-PROFIT CORPORATION

Typeset in LaTeX

Copyright ©2011 by Mathematical Sciences Publishers

Journal of Mechanics of Materials and Structures

Volume 6, No. 9-10 November–December 2011

Turtle shell and mammal skull resistance to fracture due to predator bites and ground impact DAVID L. HU, KELLY SIELERT and MICHAEL GORDON 1197

Linear buckling analysis of cracked plates by SFEM and XFEM P. M. BAIZ, S. NATARAJAN, S. P. A. BORDAS, P. KERFRIDEN and T. RABCZUK 1213

A finite element for form-finding and static analysis of tensegrity structures DARIO GASPARINI, KATALIN K. KLINKA and VINICIUS F. ARCARO 1239

Structural design of pyramidal truss core sandwich beams loaded in 3-point bending MING LI, LINZHI WU, LI MA, BING WANG and ZHENGXI GUAN 1255

Wave scattering from a rectangular crack in an anisotropic cladding PER-ÅKE JANSSON 1267

Effect of adding crumb tire rubber particles on the mechanical properties of DCPD-modified sulfur polymer mortars HAMED MARAGHECHI, IMAN FOTOVAT AHMADI and SIAMAK MOTAHARI 1283

Uniqueness theorems in the equilibrium theory of thermoelasticity with microtemperatures for microstretch solids ANTONIO SCALIA and MERAB SVANADZE 1295

Implications of shakedown for design of actively cooled thermostructural panels NATASHA VERMAAK, LORENZO VALDEVIT, ANTHONY G. EVANS, FRANK W. ZOK and ROBERT M. MCMEEKING 1313

1559-3959(2011)6:9;1-7